Local distortions in multiferroic $AgCrO_2$ triangular spin lattice

A. M. L. Lopes,[1,*] G. N. P. Oliveira,[1] T. M. Mendonça,[2] J. Agostinho Moreira,[2] A. Almeida,[2] J. P. Araújo,[2] V. S. Amaral,[3] and J. G. Correia[1,4]

[1]*Centro de Física Nuclear, Universidade de Lisboa, Av. Prof. Gama Pinto, 2, 1649-003 Lisboa, Portugal*

[2]*Instituto de Nanociência e Nanotecnologia, Universidade do Porto, Rua do Campo Alegre, 687, 4169-007 Porto, Portugal*

[3]*Departamento de Física e CICECO, Universidade de Aveiro, Campus Universitário de Santiago, 3810-193 Aveiro, Portugal*

[4]*Instituto Tecnológico e Nuclear, EN 10 - Apartado 21, 2686-953 Sacavém, Portugal*

(Received 20 March 2011; published 29 July 2011)

In this work an electric-field gradient and magnetic hyperfine field study of the multiferroic $AgCrO_2$ triangular spin lattice is presented. Perturbed angular correlation measurements at different temperatures, revealed the coexistence of two electric-field gradients, i.e., two distinct local environments at temperatures below 100 K. The emerging second local environment appears as a distortion of the Cr surrounding resulting in a local symmetry lowering. This local distortion emerges much above T_N and concomitantly with the onset of short-range magnetic correlations. We claim that, through a magnetoelastic instability, distinct Cr-Cr exchange interaction pathways appear providing a channel for magnetic frustration release.

DOI: 10.1103/PhysRevB.84.014434 PACS number(s): 75.85.+t, 76.80.+y, 75.47.Lx, 77.80.−e

I. INTRODUCTION

Magnetoelectric materials experienced a renewed interest in the last decade. Their enhanced multifunctional physical properties are extremely appealing for technological applications into memories that could be written electrically and read magnetically, or vice versa.[1–5] Recently, delafossite materials such as $CuCrO_2$ and $AgCrO_2$ just enlarged the number of systems presenting simultaneously magnetic and ferroelectric orders.[6] It has also been found that these systems present an outstanding tunability of the ferroelectric polarization by the magnetic field.[7] Moreover, the impact in the magnetoelectric coupling of their peculiar triangular spin arrangement is now under thorough examination.[7–12]

The $A^{1+}Cr^{3+}O_2^{2-}$ (A = Ag, Cu, Pd) system crystallizes in a rhomboedric layered structure within the $R\bar{3}m$ space group. The Cr spins ($3d^3$, $S = 3/2$) form an equilateral triangular lattice where the direct hybridization of the in-plane Cr d orbitals (t_{2g}) leads to strong antiferromagnetic exchange interactions.[6] Thus these materials resemble the two-dimensional (2D) Heisenberg triangular spin systems where its microscopically degenerated ground state inhibits the realization of a macroscopic magnetic order and only short-range correlations are usually observed. Nevertheless, in these delafossite systems, frustration can be, at least, partially, lifted through a 120° spin spiral magnetic order or by an incommensurate spin order, as recently suggested by neutron powder-diffraction studies in $CuCrO_2$.[13] Also, the entanglement of spin-lattice degrees of freedom can provide a channel for frustration release through lattice distortions as observed in 3D frustrated pyrochlore spinels such as $ZnCr_2O_4$ (Ref. 14) or $KFe(MoO_4)_2$.[15] In a similar manner, crystal symmetry lowering is claimed to be responsible for degeneracy lift in frustrated $CuCrS_2$ (Ref. 16) and $CuFeO_2$ (Ref. 17) delafossites.

The magnetoelectric coupling in these frustrated spin systems challenges conventional theories.[12] Although few theoretical frameworks have been brought forward,[8,10–12,18] a better knowledge on this subject is being prevented by the lack of information on the local perturbations of the periodic magnetic and structural landscape. In fact, hidden structural details coupled to spin order were just revealed through a magnetostriction study in $CuCrO_2$ single crystals.[19,20]

Aiming to unveil possible local distortions, as well as their correlations with the magnetic and/or electric orders, we undertook a detailed local probe study in the $AgCrO_2$ delafossite system. Through the temperature evolution of the electrical-field gradient (efg) we were able to observe that, not only are local distortions in fact present in $AgCrO_2$, but they appear considerably above T_N. The onset of these structural instabilities with consequent local rhombohedral symmetry breaking is discussed.

II. EXPERIMENTAL METHODS

The single-phase polycrystalline sample used in this work has been prepared by a standard solid-state reaction method where a stoichiometric mixture of $AgNO_3$ and Cr_2O_3 was used as the starting material. The final sintering treatments were performed at 1173 K under oxygen flow. In order to check the sample quality a structural, magnetic, and dielectric characterization was performed after sample preparation. The x-ray powder pattern was collected using a Siemens D5000 diffractometer with Cu K_α radiation. The diffractograms were obtained at room temperature in a $10^\circ < 2\theta < 100^\circ$ range. The magnetic susceptibility measurements in the 10–300-K temperature range, carried out using a commercial superconducting quantum interference device (SQUID) magnetometer, were performed under a $H = 100$ Oe magnetic field using the zero-field-cooling procedure. Dielectric permittivity measurements were performed at 1 MHz frequency, from 10 to 300 K, in cooling and heating runs. To perform the efg measurements, meaning γ-γ perturbed angular correlations (PAC) measurements, the sample was implanted with ^{111}In ions ($^{111}In \rightarrow {}^{111}Cd$, $t_{1/2} = 2.8$ d) to a small dose of 10^{11} at./cm^2 (dose lower than 1 ppm of the Cr/Ag concentration) and 30 keV energy at the ISOLDE/CERN facility. To fully recover from remaining implantation damage the sample was then annealed for 20 min at 973 K in oxygen flow. PAC

measurements performed in the 12–450-K temperature range were carried out on a 6-BaF_2-detector spectrometer.[21] The experimental $R(t)$ anisotropy function was obtained and the perturbation factor $G_{kk}(t)$ was extracted:

$$R(t) = A_{kk}G_{kk}(t) = A_{kk}\left(S_{k0} + \sum_n \cos(w_n t)e^{-\delta\omega_n t}\right), \quad (1)$$

where $G_{kk}(t)$ contains the signature of the lattice field interacting with the probes and the A_{kk} coefficients depend only on the nuclear cascade. Note that $G_{kk}(t)$ is here expressed for the particular case of a pure and static electric quadrupolar interaction. The transition frequencies ω_n with relative width δ and correspondent amplitudes S_{kn} are determined by the diagonalization of the hyperfine interaction Hamiltonian.[22] In the particular case of spin $I = 5/2$ and for a pure quadrupolar interaction, three transition frequencies are observable per efg. The ω_n frequencies are related to the principal component of the efg tensor V_{zz} and to the axial asymmetry parameter η, where $\eta = \frac{V_{xx}-V_{yy}}{V_{zz}}$.[22] These two parameters, V_{zz} and η, fully characterize the efg tensor. It is also convenient to define the fundamental quadrupolar frequency,

$$\omega_0 = \frac{6eQV_{zz}}{4I(2I-1)\hbar}, \quad (2)$$

since in the particular case of $\eta = 0$ the fundamental quadrupolar frequency matches the lower observable, i.e., $\omega_1 = \omega_0$ being $\omega_2 = 2\omega_0$ and $\omega_3 = 3\omega_0$. In Eq. (2), Q stands for the nucleus electrical quadrupolar moment. When both magnetic and electric interactions are present, Eq. (1) has to be modified to account for such combined static interaction. In addition to the quadrupolar frequency a Larmor frequency $\omega_L = \gamma\ B_{hf}$, corresponding to the magnetic interaction, should be defined, where γ is the gyromagnetic ratio and B_{hf} is the magnitude of the magnetic hyperfine field (mhf).

III. RESULTS AND DISCUSSION

The x-ray powder pattern, collected at room temperature, showed reflections belonging to the delafossite structure, i.e., the sample is characterized by a single crystallographic phase with rhombohedral symmetry ($R\bar{3}m$ space group). The lattice parameters obtained by x-ray pattern refinement held $a = b =$ 2.986(3) Å and $c = 18.509(4)$ Å, in very good agreement with literature.[23]

In Fig. 1 (top) the temperature dependence of the reciprocal magnetic susceptibility data with a linear fit to the paramagnetic region is presented. In the inset the susceptibility temperature derivative is shown. The magnetization measurements evidenced a paramagnetic to antiferromagnetic phase transition, taken from the maximum of susceptibility temperature derivative, around $T_N = 21$ K. The Curie-Weiss temperature was found to be $\Theta_P = -185(15)$ K, which leads to $\Theta_P/T_N = 9$, confirming the high degree of frustration of the system. Also, taken from the linear part of the reciprocal susceptibility, an effective paramagnetic moment of $3.7\mu_B$ was obtained. Moreover, below approximately $T = 100$ K a clear deviation from the Curie-Weiss law was observed. This magnetic anomalous behavior, reported also for other

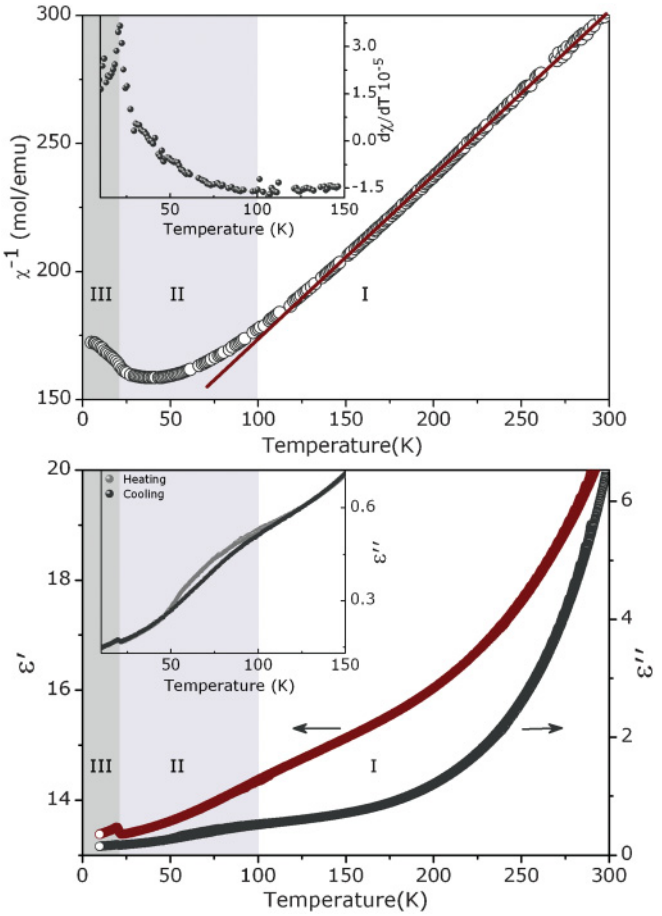

FIG. 1. (Color online) Top: $AgCrO_2$ reciprocal magnetic susceptibility data as a function of temperature measured at 100 Oe, from 5 to 300 K. In the reciprocal magnetic susceptibility data the linear fit to the paramagnetic region is also presented. The three signed regions stand for I, paramagnetic; II, 2D magnetic correlations; and III, antiferromagnetic and ferroelectric. The inset depicts the reciprocal magnetic susceptibility temperature derivative in the 10–150 K temperature range. Bottom: temperature dependence of both real (ϵ') and imaginary (ϵ'') parts of the complex dielectric constant, measured at 1 MHz, from 10 to 300 K, in both cooling and heating runs. The inset depicts a detail of the dielectric permittivity imaginary part ϵ'' in the 10–150 K temperature range, in both cooling and heating runs.

$ACrO_2$ delafossites, has been attributed to the development of 2D short-range magnetic correlations.[24] According to these results the three signed regions in Fig. 1 and figures below stand for I: paramagnetic; II: 2D magnetic correlations; and III: antiferromagnetic phases.

Figure 1 (bottom) depicts the temperature dependence of both real (ϵ') and imaginary (ϵ'') parts of the complex dielectric constant, measured at 1 MHz, in both cooling and heating runs. The inset shows a magnification of the temperature dependence of the imaginary part of the dielectric constant ϵ'' in the 10–150-K temperature range, measured in cooling and heating runs. Anomalies in both $\epsilon'(T)$ and $\epsilon''(T)$ observed at $T_N = 21$ K mark the ferroelectric phase transition.[6] Moreover, other significant features deserve to be outlined, namely the very broad anomaly emerging below 125 K, and the distinct

difference in the shape of $\epsilon''(T)$ regarding cooling and heating runs (see inset). The nature of this anomaly will be discussed later in the text together with the efg results.

Figure 2 depicts representative PAC spectra and correspondent fits [continuous lines over the $R(t)$], obtained in the 12–450-K temperature range for the $AgCrO_2$ system. In the same figure, the Fourier transforms of the $R(t)$ functions are presented. At high temperatures, $T > 100$ K, a frequency triplet (ω_1, ω_2, and ω_3 with $\omega_2 \sim 2\omega_1$ and $\omega_3 \sim 3\omega_1$) corresponding to a single efg can be clearly observed. By a simple picture inspection one can realize that in this temperature range no significant changes occur in the spectra when the temperature is lowered and only one efg, i.e., one probe local environment, exists. However, below 100 K visible changes can be observed in the $R(t)$ data and correspondent Fourier transforms. In detail, a second efg emerges and its relative abundance increases with decreasing temperature. Accordingly, the fits to the $R(t)$ experimental data were performed considering only one static efg distribution, which was assumed to be Lorentzian-like, for $T \geqslant 100$ K while two efg distributions had to be considered to account for the features that emerge below that temperature.

The spectrum obtained at room temperature revealed an efg characterized by a fundamental frequency of $\omega_0^u = 123(1)$ Mrad/s ($V_{zz}^u = 6.54 \times 10^{21}$ V/m^2) and an asymmetry parameter $\eta^u = 0.0(1)$ in good agreement with literature.[25] The second efg that emerges below 100 K is characterized by a similar fundamental frequency, $\omega_0^d = 125(2)$ Mrad/s ($V_{zz}^d = 6.84 \times 10^{21}$ V/m^2), and an asymmetry parameter $\eta^d = 0.5(1)$.

The thermal dependence of the efgs parameters $V_{zz}^{u,d}$ and $\eta^{u,d}$ are depicted in Fig. 3. As can be seen, the efg parameters of both efg^u and efg^d increase slightly as the temperature decreases toward $T_N = 21$ K. However, below T_N a steep increase of those parameters is observable for the (d) second local environment. One should also mention that the relative widths of the efg distributions are nearly temperature independent ($\delta^u \approx 2$ Mrad/s and $\delta^d \approx 8$ Mrad/s).

Figure 4 presents the temperature evolution of the fraction of probes interacting with each efg, i.e., the relative abundance of each local environment (LE): f^u and f^d. As depicted, at high temperatures all the probes interact with efg^u. On decreasing temperature and below 100 K, a second efg, efg^d, becomes apparent. Below that temperature f^u decreases sharply and seems to vanish for temperatures below 12 K. Also, it can be seen that at T_N, $f^u \approx f^d \approx 48$ (8)%.

Before analyzing the nature of the each LE and their temperature evolution one should first mention that symmetry arguments, efg calculations and measurements in similar systems,[25,26] have shown that efg^u is only compatible with probes substituting the trivalent B site, i.e., the Cr site. Moreover, considering that at temperatures as low as 100 K the probes do not change their location (e.g., probe ions diffusion), the efg^d can therefore only be associated with modifications in the Cr/probe local environment. Comparing these two LEs one realizes that the most relevant difference between efg^u and efg^d is their asymmetry parameter. While efg^u is axial symmetric, $\eta^u \approx 0$, efg^d is a nonaxial symmetric local environment, $\eta^d \approx 0.5$. As a consequence, while part of the system (associated with efg^u) maintains its local rhombohedral symmetry, the

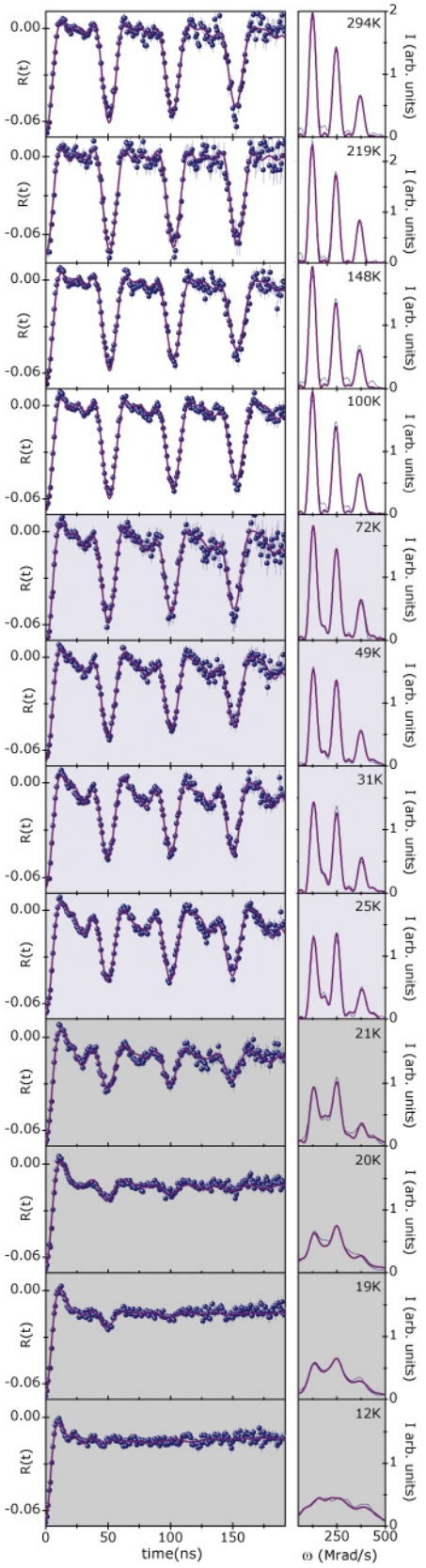

FIG. 2. (Color online) Representative $R(t)$ experimental functions (dots) and corresponding fits (lines) obtained for the $AgCrO_2$ system at different temperatures. Corresponding Fourier transforms are displayed on the right side.

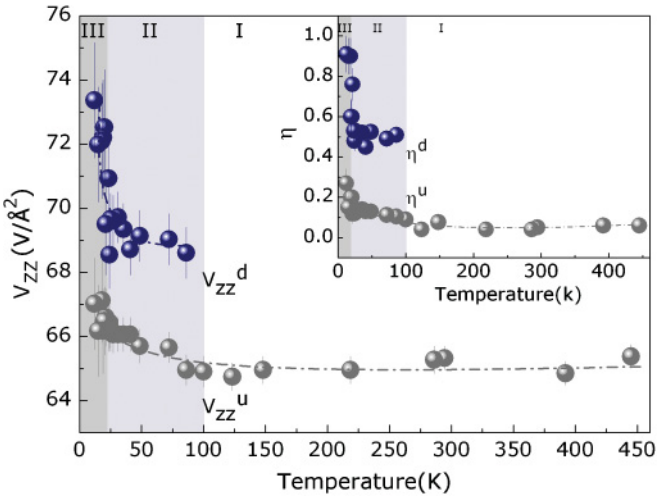

FIG. 3. (Color online) efg principal component V_{zz} and asymmetry parameter η (inset) for the f_u and f_d local environments as a function of temperature. Lines are guides for the eye. Regions I, II, III as defined in Fig. 1.

remaining part, associated with efg^d, appears as a distortion of the first, with axial symmetry breaking.

As mentioned above the ^{111}Cd probe state is fed by the ^{111}In radioactive decay. This process occurs through electron capture (EC) of an electron from the probe K shell. An electron-shell recombination follows the EC decay and leaves the probe in a highly ionized state. The inner electron shells are filled much too fast to have an effect on the PAC spectra.[27,28] However, the recovery rates of the outer shells and their nearest-neighbor ions toward the equilibrium electronic configuration can be, in particular cases (insulators and wide-band-gap semiconductors) of the same order of the PAC time scale (10^{-9}–10^{-6} ns). This slow re-arrangement of the probe and neighborhood atoms to a final stable configuration (so-called after effects) can, sometimes, affect the experimental PAC function. The existence of spectra features due to after effects on the present experiments should be, however, excluded. After effects account for transient efg's

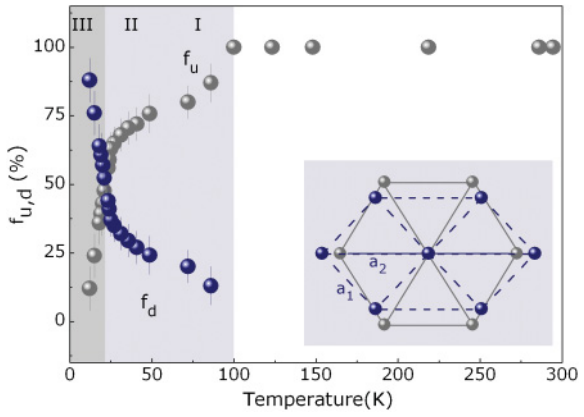

FIG. 4. (Color online) Temperature dependence of the probe fractions f_u and f_d. Inset; schematic representation of an in-plane distortion of the equilateral Cr lattice. Regions I, II, III as defined in Fig. 1.

due to delayed electron-shell recombination. The main effect expected on the PAC spectra would be a situation described by time-dependent hyperfine interactions, in particular, described by a unidirectional relaxation process.[28,29] This describes the stochastic transition from an initial "unfilled" state to a final stable one after electron recombination. The initial state would mostly be described by a strongly damped efg distribution and the final one by an unperturbed, well defined, efg. In fact, this leads mainly to a constant reduction of the PAC spectra amplitude, for times longer then a few ns, but with unchanged features apart from that reduction (unchanged quadrupole parameters). Such is not the case of the present data with a phenomenology consistent with the material's intrinsic properties. Other dynamics effects, such intrinsic or extrinsic equilibrium efg fluctuations, should[30,31] also be excluded from the interpretation since no exponential damping growth is observed at any temperature. On the other hand, in this system's local distortions have been theoretically predicted and experimentally observed below T_N.[16,19,20] Thus below that temperature a second efg and a mhf is expected. The fits below T_N have been perfectly performed with the inclusion of typical combined interactions. These materials are narrow-band-gap semiconductors, in particular $AgCrO_2$ has a 1.68-eV band gap,[23] that might be the reason why after effects are not observable on these experiments.

Here it also should be stressed that the observed distortions are also witnessed by the dielectric permittivity results. Specifically, the very broad anomaly emerging below 125 K and the distinct difference in shape of $\epsilon''(T)$, regarding cooling and heating runs, point to slight charge dislocations below that temperature. Moreover, those results are favorable for the presence of a nonergodic, frustrated state in the temperature range T_N–125 K, where long-range ordering does not prevail. This statement entirely corroborates the results obtained from PAC and magnetization data. Furthermore, the quite good agreement between dielectric and magnetization data to understand the behavior of $AgCrO_2$ is still an evidence for the existence of a magnetodielectric coupling in this compound. Analyzing together the magnetic susceptibility, complex dielectric permittivity, and the efg data, it is evident that the above-mentioned high-temperature anomaly in the magnetization appears along with the anomaly in the dielectric permittivity data and with the onset of the efg^d. This result suggests that the observed distortions are linked to the magnetic degrees of freedom. In particular, the development of such local distortions should be related to the onset of short-range magnetic correlations, i.e., a magnetoelastic coupling seems to drive the system to lower symmetry. When lowering the temperature, the number of distorted places increases and eventually, when $f_d = 48(8)\%$, the 3D magnetic order and ferroelectric transition is attained.

Recent magnetostriction studies in the isostructural $CuCrO_2$ presented evidences for lattice distortion with crystallographic symmetry lowering below T_N. In that work, an in-plane deformation of the equilateral Cr triangular lattice coupled to magnetic order has been suggested.[19] These findings have been supported by magnetization and high-field multifrequency ESR measurements where the experimental data have been modeled with a 118° spiral spin structure on a distorted Cr triangular lattice.[20]

To correlate possible Cr triangular lattice distortion with the efg^d obtained in this work, point-charge model efg calculations, using the first shells atoms (O, Cr, and Ag), have been performed. Note that such simple calculation, after proper Sternheimer corrections,[32] held a fair efg estimate for the undistorted rhombohedral lattice (efg^u): $V_{zz}^{calc} = 6.9 \times 10^{21}$ V/m^2 and $\eta = 0$ (atomic positions and cell parameters taken from Gehle *et al.*[33]). Before continuing one should remind that the most relevant difference between efg^u and efg^d is the loss of axial symmetry ($\eta \neq 0$). With this in mind, and in an attempt to simulate the experimental efg^d, the Cr triangular lattice was distorted in a way that $(a_2 - a_1)/a_1 \neq 0$, $V_{zz}^{calc} = V_{zz}^{d}$, and $\eta^{calc} \neq 0$. Once the trigonal symmetry is broken η departs from zero, but even for $(a_2 - a_1)/a_1 \approx 10^{-2}$, η^{calc} is extremely small. A calculation with in-plane distortion of all atoms held a higher η, nevertheless, still far from the experimental one, $\eta^d = 0.5$. Thus according to our results the low-temperature distortions in the $AgCrO_2$ system seem to be more complex than a simple in-plane distortion of the equilateral Cr lattice and should involve also out-of-plane chromium and/or oxygen atoms distortions. Note that the establishment of the 3D magnetic order in these systems is being discussed in terms of the delicate balance between the nearest- and next-nearest-neighbor's intra- and interlayer exchange interactions.[10,11,34] Though more accurate simulations are necessary to unveil the type of distortion that is behind efg^d, our results should be taken into consideration when modeling this system.

We now analyze in more detail the results below T_N. As one can observe in Fig. 2, below T_N a damping of the perturbation function, $R(t)$, and a corresponding line broadening in the Fourier spectra are clearly observed. As the temperature decreases, these features become more evident and at 12 K a complete damping of the $R(t)$ experimental data is observed. This result is due to the presence of a combined interaction (electric and magnetic hyperfine interaction). Thus below T_N the $R(t)$ experimental data also show the presence of hyperfine fields due to the antiferromagnetic ordering. Close to T_N when the magnetic hyperfine field interaction is much weaker than the electric quadrupole one, only a frequency broadening is observed. Lowering the temperature, the magnetic hyperfine interaction progressively overcomes the electric quadrupole interaction and in this case the combined interaction completely damps the $R(t)$ experimental data, as observed at 12 K.

To perform the low-temperature PAC fits the spin arrangement proposed by Oohara and co-workers for $AgCrO_2$ (Ref. 24) and by Kadowaki and Ajiro for $CuCrO_2$ (Ref. 35) was considered as a starting model. Within this magnetic arrangement the spins on the in-plane Cr triangular lattice form a 120° angle with each other and thus two magnetic nonequivalent probe lattice sites exist; see Fig. 5. In the type-I magnetic environment the probe replaces the atom with spin along the c-axis direction while in type II the probe replaces one of the spins oriented approximately 120° from the c axis. In both cases and due to the nearest-neighbor uncompensated spins a sizable mhf should be measured. Since there are two high-temperature local environments, LE$_u$ (undistorted, $\eta = 0$) and LE$_d$ (distorted, $\eta \neq 0$), and a two-spin arrangement,

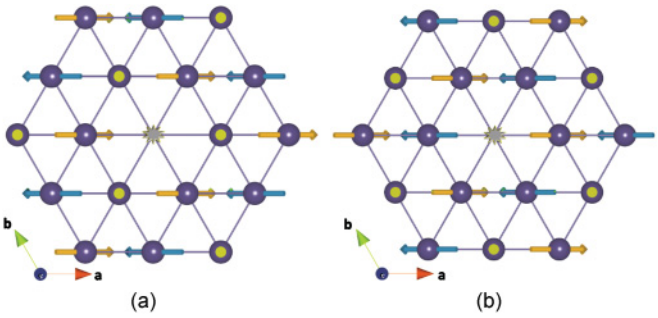

FIG. 5. (Color online) Two possible spins configurations surrounding the PAC probe (center of the hexagon) in the $AgCrO_2$ triangular Cr planes. (a) In type-I magnetic environment the probe replaces the atom with spin along the c-axis direction. (b) In type II the probe replaces one of the spins oriented 120° from the c axis.

four combined interactions should be used to perform the fits. Nevertheless, it was verified that in the undistorted environment, LE$_u$, the magnetic hyperfine field is too small to resolve the two distinct mhf orientations. Moreover, it was observed that for the distorted environment, mhf^{d1} and mhf^{d2} differ essentially on their orientation, their magnitude being approximately the same ($B_{hf}^{d1} \approx B_{hf}^{d2}$). The final $R(t)$ spectra fits were performed accordingly.

In Fig. 6 the mhf parameters, B_{hf}^{u}, B_{hf}^{d}, temperature evolution, for LE$_u$ and LE$_d$, are shown. As one can observe a small magnetic hyperfine field is detected at 24 K for LE$_d$; this suggests that a local spontaneous magnetic order might exist already at that temperature. This observation is in agreement with former neutron-diffraction measurements that have shown a similar result.[24] As depicted in Fig. 6, the mhf magnitude in the undistorted LE attains, at low temperatures, a small value around $B_{hf}^{u} = 0.9(4)$ T. Given the mhf^u magnitude, an accurate determination of the angle β_{hf}^{u} was not possible. For the distorted LE, LE$_d$, a clear increase of the mhf^d magnitude reaching a value of $B_{hf}^{d} = 6.9(6)$ T at 12 K is observed. The angles between the mhf and the principal component of the efg were found to be nearly temperature

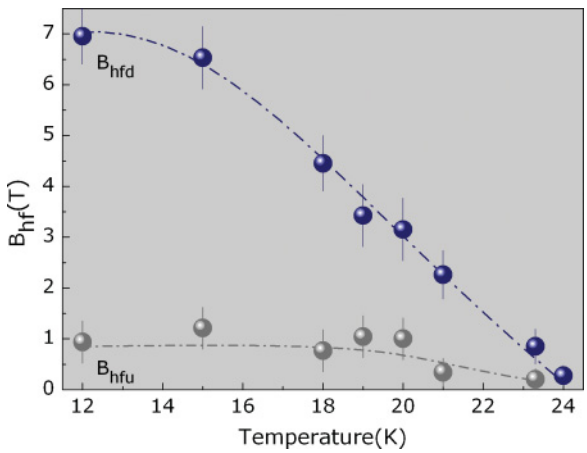

FIG. 6. (Color online) Magnetic hyperfine field as a function of temperature for the undistorted, B_{hf}^{u}, and distorted, B_{hf}^{d}, local environment. Lines are guides for the eyes.

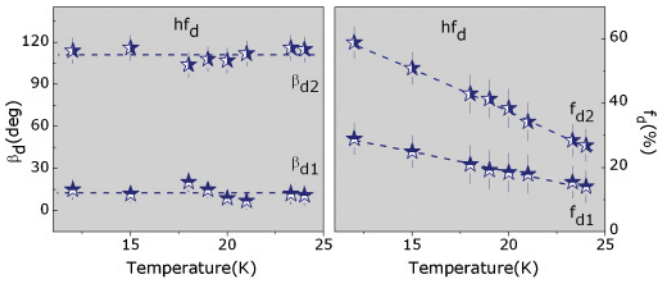

FIG. 7. (Color online) (left) Angle between the efg principal component and mhf as a function of temperature for the distorted environment. (right) Probe distribution among the distorted environment as a function of temperature. Lines are guides for the eyes.

independent and around $\beta_{hf}^{d1} = 112(8)^\circ$ and $\beta_{hf}^{d2} = 13(6)^\circ$ (see Fig. 7). In Fig. 7 the fraction of probes, f_{d1} and f_{d2}, in the distorted LE ($f_d = f_{d1} + f_{d2}$) experiencing mhf^{d1} (f_{d1}) and mhf^{d2} (f_{d2}) are also shown. As one can see, the temperature dependence of f_{d1} and f_{d2} roughly respects the relation $f_{d1} = 2f_{d2}$, as expected by magnetic symmetry.

As mentioned above, frustrated magnetic lattices usually do not survive in the low-temperature limit and lattice distortions; exotic spin configurations or charge disproportionation might lift the degeneracy. In a similar manner, here, the observed local distortions, corroborated by the broad anomaly in the complex dielectric constant, are linked to the magnetic degrees of freedom. In particular, the appearance of the structural deformations below 100 K are related with the onset of short-range magnetic correlations occurring well above T_N and evidenced in our susceptibility data. Our data are compatible with a scenario where at the onset of the short-range magnetic correlations, $T \approx 100$ K, a magnetoelastic instability occurs and local distortions, breaking the axial symmetry, appear as a channel for frustration release. These distortions lead to a nonuniform pattern of nearest-neighbor Cr-Cr exchange interactions allowing a degeneracy lift. According to our results the 3D magnetic order within a ferroelectric lattice is attained when the fraction of distorted environments reaches values around 48(8)%. In the magnetic ordered phase the number of distorted sites continues to increase and at 12 K only 10(6)% of the local environments maintain its high-temperature symmetry. The remaining LE experience also, on decreasing temperature below T_N, a steep increase in its efg parameters, which might be related to the reported increase of electrical polarization.[6] In ferroelectric materials, the efg temperature dependence is usually associated with two main contributions: a weak temperature dependence due to the rigid lattice expansion and a stronger contribution due to ferroelectric displacements. In fact, it has been shown that the V_{zz} temperature dependence in a ferroelectric phase is dominated by the square of the spontaneous lattice polarization.[36–38] Moreover, an increasing local magnetic field, reaching $B_{hf}^{d} = 6.9(6)$ T at 12 K, compatible with the mentioned spin model and with the magnetoelectric nature of this system, is observed in the distorted LE. On the other hand, only a small mhf is measured in the rhombohedral (undistorted) local environment. This result may suggest that, contrary to what is observed in the distorted phase, the absence of the local distortions might inhibit the frustration release at these sites. The residual mhf, observed in the LE^d, could arise via a second-neighbor or interplane exchange interactions.

IV. CONCLUSIONS

In summary, the $AgCrO_2$ local structure was followed through the temperature evolution of the electrical-field gradient and magnetic hyperfine field. These data were correlated with complementary magnetization and complex dielectric permittivity measurement. We give evidences that at $T \approx 100$ K and concomitantly with the onset of short-range magnetic correlations, a local distortion of the Cr surrounding emerges. We show that lowering the temperature below 100 K, and still above T_N, part of the system loses the local rhombohedral symmetry. This symmetry lowering is associated to the coupling between the elastic and magnetic degrees of freedom that provide a channel for magnetic frustration release through a lattice distortion. Though we cannot ascertain the detailed nature of the new structure, we argue that the distortions in the $AgCrO_2$ system are not a simple deformation of the equilateral Cr lattice into an in-plane isosceles configuration. Additional measurements and efg calculations with complementary techniques are now necessary to unveil the details of the observed distortion and thus give a step forward to a comprehensive understanding of these exquisite systems.

ACKNOWLEDGMENTS

This work was supported by Portuguese Foundation for Science and Technology (Projects No. CERN/FP/109357/2009, No. CERN/FP/116320/2010, and No. PTDC/FIS/105416/2008), European Union with FP7 through ENSAR (Contract No. 262010), German BMBF (Contract No. 05KK7TS2), and ISOLDE Collaboration (Project No. IS487).

*Present address: CFNUL, Centro de Física Nuclear, Universidade de Lisboa, Av. Prof. Gama Pinto, 2, 1649-003 Lisboa, Portugal; armandina.lima.lopes@cern.ch

[1] M. Bibes and A. Barthelemy, Nat. Mater. **7**, 425 (2008).
[2] S. H. Baek *et al.*, Nat. Mater. **9**, 309 (2010).
[3] K. F. Wang, J. M. Liu, and Z. F. Ren, Adv. Phys. **58**, 321 (2009).
[4] W. Kleemann, Physics **2**, 105 (2009).
[5] D. Khomskii, Physics **2**, 20 (2009).
[6] S. Seki, Y. Onose, and Y. Tokura, Phys. Rev. Lett. **101**, 067204 (2008).
[7] K. Kimura, H. Nakamura, S. Kimura, M. Hagiwara, and T. Kimura, Phys. Rev. Lett. **103**, 107201 (2009).
[8] Y. Tokura and S. Seki, Adv. Mater. **22**, 1554 (2010).
[9] S. Seki, H. Murakawa, Y. Onose, and Y. Tokura, Phys. Rev. Lett. **103**, 237601 (2009).

[10]M. Poienar, F. Damay, C. Martin, J. Robert, and S. Petit, Phys. Rev. B **81**, 104411 (2010).
[11]E. J. Kan, H. J. Xiang, Y. Zhang, C. Lee, and M.-H. Whangbo, Phys. Rev. B **80**, 104417 (2009).
[12]S. Ishihara, J. Phys. Soc. Jpn. **79**, 011010 (2010).
[13]M. Poienar, F. Damay, C. Martin, V. Hardy, A. Maignan, and G. André, Phys. Rev. B **79**, 014412 (2009).
[14]S. Ji, S.-H. Lee, C. Broholm, T. Y. Koo, W. Ratcliff, S.-W. Cheong, and P. Zschack, Phys. Rev. Lett. **103**, 037201 (2009).
[15]A. I. Smirnov *et al.*, Phys. Rev. Lett. **102**, 037202 (2009).
[16]J. C. E. Rasch, M. Boehm, C. Ritter, H. Mutka, J. Schefer, L. Keller, G. M. Abramova, A. Cervellino, and J. F. Löffler, Phys. Rev. B **80**, 104431 (2009).
[17]F. Ye, Y. Ren, Q. Huang, J. A. Fernandez-Baca, P. Dai, J. W. Lynn, and T. Kimura, Phys. Rev. B **73**, 220404 (2006).
[18]C. D. Hu, Phys. Rev. B **81**, 224414 (2010).
[19]K. Kimura, T. Otani, H. Nakamura, Y. Wakabayashi, and T. Kimura, J. Phys. Soc. Jpn. **78**, 113710 (2009).
[20]H. Yamaguchi, S. Ohtomo, S. Kimura, M. Hagiwara, K. Kimura, T. Kimura, T. Okuda, and K. Kindo, Phys. Rev. B **81**, 033104 (2010).
[21]T. Butz, S. Saibene, T. Fraenzke, and M. Weber, Nucl. Instrum. Methods, Phys. Res. A **284**, 417 (1989).
[22]G. Schatz and A. Weidinger, *Nuclear Condensed Matter Physics: Methods and Applications* (John Wiley and Sons Ltd., Sussex, 1996).
[23]S. Ouyang, Z. Li, Z. Ouyang, T. Yu, J. Ye, and Z. Zou, J. Phys. Chem. C **112**, 3134 (2008).
[24]Y. Oohara, S. Mitsuda, H. Yoshizawa, N. Yaguchi, H. Kuriyama, T. Asano, and M. Mekata, J. Phys. Soc. Jpn. **63**, 847 (1994).
[25]R. N. Attili, M. Uhrmacher, K. P. Lieb, L. Ziegeler, M. Mekata, and E. Schwarzmann, Phys. Rev. B **53**, 600 (1996).
[26]R. N. Attili, R. N. Saxena, A. W. Carbonari, J. M. Filho, M. Uhrmacher, and K. P. Lieb, Phys. Rev. B **58**, 2563 (1998).
[27]O. Keski-Rahkonen and M. Krause, At. Data Nucl. Data Tables **14**, 139 (1974).
[28]D. Lupascu, S. Habenicht, K.-P. Lieb, M. Neubauer, M. Uhrmacher, and T. Wenzel, Phys. Rev. B **54**, 871 (1996).
[29]S. Habenicht, D. Lupascu, M. Uhrmacher, L. Ziegeler, and K.-P. Lieb, Z. Phys. B **101**, 187 (1996).
[30]A. M. L. Lopes, J. P. Araújo, J. J. Ramasco, E. Rita, V. S. Amaral, J. G. Correia, and R. Suryanarayanan, Phys. Rev. B **73**, 100408 (2006).
[31]M. Neubauer, A. Bartos, K. P. Lieb, D. Lupascu, M. Uhrmacher, and T. Wenzel, Europhys. Lett. **29**, 175 (1995).
[32]F. D. Feiock and W. R. Johnson, Phys. Rev. **187**, 39 (1969).
[33]E. Gehle and H. Sabrowsky, Z. Naturforsch. B **30**, 659 (1975).
[34]R. S. Fishman, Phys. Rev. Lett. **106**, 037206 (2011).
[35]H. K. H Kadowaki and Y. Ajiro, J. Phys.: Condens. Matter **2**, 4485 (1990).
[36]Y. Yeshurun, S. Havlin, and Y. Schlesinger, Solid State Commun. **27**, 181 (1978).
[37]V. G. Bhide and M. S. Multani, Phys. Rev. **139**, A1983 (1965).
[38]M. Löhnert, G. Kaindl, G. Wortmann, and D. Salomon, Phys. Rev. Lett. **47**, 194 (1981).